Molecular Detection of SARS-CoV-2 Infection in FFPE Samples and Histopathologic Findings in Fatal SARS-CoV-2 Cases

Miroslav Sekulic, MD,[1,2,*] *Holly Harper, MD,*[1,2,*] *Behtash G Nezami, MD,*[1,2] *Daniel L. Shen, MD,*[1,2] *Simona Pichler Sekulic, MD,*[1,2] *Aaron T. Koeth, BMS,*[1] *Clifford V Harding, MD, PhD,*[1,2] *Hannah Gilmore, MD,*[1,2] *and Navid Sadri, MD, PhD*[1,2]

From the [1]Department of Pathology, University Hospitals Cleveland Medical Center, Cleveland, OH; and [2]Department of Pathology, Case Western Reserve University School of Medicine, Cleveland, OH.

Key Words: COVID-19; nCov-19; FFPE; Autopsy; Molecular testing; Viral sequencing; SARS-CoV-2; Coronavirus

Am J Clin Pathol 2020;XX:0–0

DOI: 10.1093/AJCP/AQAA091

ABSTRACT

Objectives: *To report methods and findings of 2 autopsies with molecular evaluation of severe acute respiratory syndrome coronavirus 2 (SARS-CoV-2) positive individuals.*

Methods: *Postmortem examination was completed following Centers for Disease Control and Prevention public guidelines. Numerous formalin-fixed paraffin-embedded (FFPE) tissue types from each case were surveyed for SARS-CoV-2 RNA by quantitative reverse transcription polymerase chain reaction (qRT-PCR). SARS-CoV-2 viral genome was sequenced by next-generation sequencing (NGS) from FFPE lung tissue blocks.*

Results: *Postmortem examinations revealed diffuse alveolar damage, while no viral-associated hepatic, cardiac, or renal damage was observed. Viral RNA was detected in lungs, bronchi, lymph nodes, and spleen in both cases using qRT-PCR method. RNA sequencing using NGS in case 1 revealed mutations most consistent with Western European Clade A2a with ORF1a L3606F mutation.*

Conclusions: *SARS-CoV-2 testing and viral sequencing can be performed from FFPE tissue. Detection and sequencing of SARS-CoV-2 in combination with morphological findings from postmortem tissue examination can aid in gaining a better understanding of the virus's pathophysiologic effects on human health.*

Key Points

- Diffuse alveolar damage is a common feature in postmortem examination of patients with severe acute respiratory syndrome coronavirus 2 (SARS-CoV-2).
- SARS-CoV-2 RNA can be detected from formalin-fixed paraffin-embedded (FFPE) blocks submitted at autopsy, with the potential to assess tissue involvement in patients with confirmed, suspected, or clinically unbeknownst infection.
- Highest SARS-CoV-2 RNA levels were observed in the lung, bronchi, lymph node, and spleen in both cases. SARS-CoV-2 genome sequencing can be done from FFPE blocks.

In December 2019, a novel severe acute respiratory syndrome coronavirus 2 (SARS-CoV-2) was identified in Wuhan, China, sparking the global coronavirus disease 2019 (COVID-19) pandemic.[1] SARS-CoV-2 is a member of the coronaviruses family, which comprises a diverse group of large, enveloped, nonsegmented, positive sense single-stranded RNA viruses.[1] Although similarities in clinical presentation exist between SARS-CoV-2 and SARS-CoV, including acute respiratory distress syndrome (ARDS) caused by diffuse alveolar damage (DAD), differences are being elucidated in the pattern and extent of major organ involvement. Studies have shown involvement of different organs in the SARS-CoV-2 disease. Despite the growing number of clinical and radiologic studies of these patients, only a few studies have so far investigated the histopathologic changes in the SARS-CoV-2 patients via biopsy and/or postmortem sampling at autopsy.[2-4] Several of these reports have

used viral culture, electron microscopy, in situ hybridization, or immunohistochemical staining to detect viral involvement in different organs. In this study we report postmortem findings and detection and sequencing of SARS-CoV-2 viral RNA from formalin-fixed paraffin-embedded (FFPE) samples of multiple organs collected in 2 patients with antemortem detection of SARS-CoV-2.

Materials and Methods

Autopsy Procedure and Histologic Examination

The decedents underwent postmortem examination following Centers for Disease Control and Prevention (CDC) public guidelines for the collection of specimens and were performed without the examination of brain or spinal cord. The lungs from case 1 were infused with formalin under gravity via the primary/main bronchi and allowed to fix for 24 hours in a container of formalin before dissection and sampling of sections. The lungs of case 2 were dissected fresh, and sampling of sections was done at the same time. For both autopsies the following organ tissues were sampled: lungs (all lung lobes), main bronchi, trachea, heart (left ventricle anterior/lateral/posterior, right ventricle, and interventricular septum), hilar and peribronchial lymph nodes, spleen, esophagus, stomach, small intestine, large intestine, liver (left and right aspects), pancreas, bilateral adrenal glands, bilateral kidneys, urinary bladder, skin, and skeletal muscle (psoas). Representative tissue samples were submitted and in standard manner formalin-fixed and paraffin-embedded. Paraffin tissue sections were stained with H&E and examined under light microscopy.

Molecular Detection of Viral RNA in FFPE Tissue

RNA was extracted from 3 unstained slides (0.5 µm thick) using Maxwell RSC RNA FFPE Kit (Promega) in elution volume of 30 µL. The CDC 2019-Novel Coronavirus Real-Time RT-PCR Diagnostic Panel assay was adapted as previously described[5] using TaqPath 1-step RT-qPCR Mastermix (Thermo Fisher), 2019-nCoV N1 and N2 primer/probe sets, and control RNAse P primer /probe set (IDT). Cycle threshold values less than 40 were considered positive. Lung tissue samples from 2 non-SARS-CoV-2 patients with DAD were run as controls and were negative.

Sequencing of SARS-CoV-2

Leftover extracted RNA used for PCR was used for sequencing with an AmpliSeq SARS-CoV-2 panel. Seven µL of RNA was converted to cDNA using SuperScript VILO III (Thermo Fisher). Library preparation was performed using AmpliSeq SARS-CoV-2 panel set and AmpliSeq Plus Library kit (Thermo Fisher). Templating was performed with Ion Chef Kit and sequencing was performed on Ion S5 Prime with Io 530 Chip Kit (Thermo Fisher). Alignment to SARS-CoV-2 reference (GenBank ID: MN908947) and variant calling was performed with Ion Torrent Suite 5.10. Variants calls were further confirmed by manual inspection using Integrative Genomics Browser (Broad Institute). Only variants with allele frequency greater than 90% were called. Genomic epidemiology classification was performed using NextStrain.org on April 27, 2020.[6]

Results

Case 1

The decedent was an 81-year-old man admitted from an assisted living facility with acute respiratory failure, fever, and positive nasopharyngeal swab SARS-CoV-2 test. Eight days prior to admission the patient was noted to have developed an afebrile cough, initially thought to be associated with congestive heart failure. Six days later, the patient was found to be febrile (38.7°C), and the following day he required 2 L/min of oxygen. Empirical management for concern of respiratory tract infection was initiated, and an outpatient nasopharyngeal swab collection for SARS-CoV-2 testing was performed. Once the patient's SARS-CoV-2 testing returned positive he was immediately admitted the same day.

The patient's medical history was otherwise notable for dementia, radiologic evidence of a left lung mass (managed with hospice care), coronary artery disease (status post coronary artery bypass grafting), atrial fibrillation (biventricular pacemaker implanted), congestive heart failure, peripheral artery disease (status post iliac stenting), diabetes mellitus, hypertension, dyslipidemia, chronic kidney disease, gout, smoking, cerebrovascular accidents, and urinary tract infections. Surgical history was further notable for carotid endarterectomy, left inguinal hernia repair, and cataract surgery.

Laboratory testing around the time of admission was notable for CBC with pancytopenia, serum creatinine of 1.55 mg/dL, blood urea nitrogen of 37 mg/dL, serum glucose of 104 mg/dL, and brain natriuretic peptide of 1,156 pg/mL. Blood and urine bacterial cultures showed no growth. Infectious disease testing was negative

DOI: 10.1093/ajcp/aqaa091

for *Legionella, Streptococcus pneumoniae,* and HIV. Body temperature was 37.8°C. Pitting edema around the ankles was noted on examination. Chest roentgenogram on the day of admission demonstrated diffuse patchy opacities in the right lung and subtle patchy opacities in the left lower lung Image 1. Chest computed tomography (CT) on the same date revealed multifocal peripheral and central ground-glass opacities throughout the bilateral lungs, a pulmonary mass in the medial aspect of the left lower lobe, small left-sided pleural effusion, moderate cardiomegaly, and calcifications of the coronary arteries and thoracic aorta.

After admission, the patient was initially given 2 L/min of oxygen via nasal cannula but began to require increasing oxygen support up to 6 L/min. The patient was also noted to have evidence of encephalopathy compounding baseline dementia. Based upon the patient's overall poor functional/physiologic status, underlying malignancy, comorbidities, and superimposed infection, it was determined that the patient's prognosis would be poor even with further management and as such, the patient was provided comfort measures. The patient was declared dead 5 days after admission, and an autopsy sine brain and spinal cord was permitted by the family. The autopsy was performed 29 hours after death.

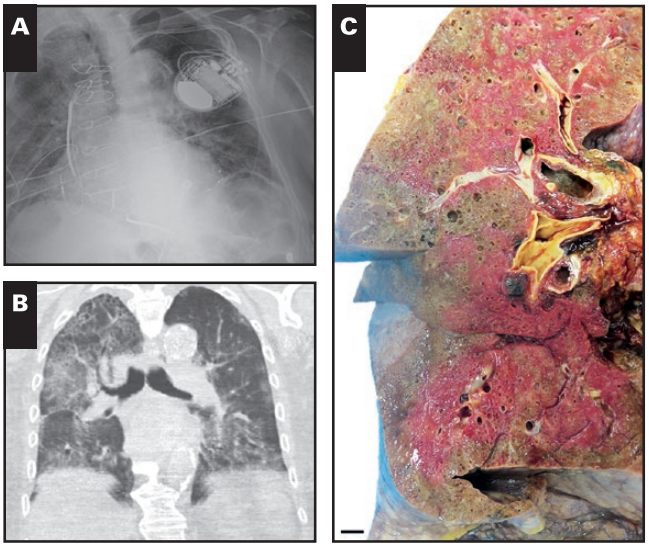

Image 1 (Case 1) Chest roentgenogram performed on the day of admission revealed diffuse patchy opacities in the right lung and subtle patchy opacities in the left lower lung (**A**), and computed tomography showed multifocal peripheral and central ground-glass opacities throughout the bilateral lungs, a pulmonary mass in the medial aspect of the left lower lobe, small left-sided pleural effusion, moderate cardiomegaly, and calcifications of the coronary arteries and thoracic aorta (**B**; the pulmonary mass and coronary artery calcifications are not present in the illustrated coronal slice). Postmortem gross examination of the right lung showed congested parenchyma superimposed on emphysematous changes (**C**; bar scale equals 1 cm; pink areas represent incomplete formalin fixation).

The postmortem gross examination of the lungs after 24 hours of inflation and submersion fixation with formalin revealed congested parenchyma superimposed on emphysematous changes, and the left lower lobe contained a mass lesion (4.5 cm in greatest dimension) Image 2. Before fixation, the right lung weighed 1,200 g, and the left lung weighed 1,040 g. Microscopically, the lungs revealed involvement of all lung lobes by acute/exudative phase of DAD characterized by hyaline membrane formation, scattered squamous metaplasia of distal airways (alveoli, alveolar ducts, and respiratory bronchioles), and background emphysematous changes (Image 2). Bronchial and tracheal sampling showed only minimal submucosal chronic inflammation with unremarkable overlying respiratory epithelium. SARS-CoV-2 RNA was detected in section of lung parenchyma, bronchi, and lymph node Table 1. The left lower lobe mass lesion was morphologically and immunophenotypically most consistent with large cell carcinoma, and there was evidence of metastatic involvement of ipsilateral hilar and peribronchial lymph nodes.

Other organs that revealed significant findings that contributed to the patient's overall physiologic status and terminal decline included the kidneys and heart. The kidneys showed evidence of acute tubular injury on a background of moderately advanced chronic changes of the renal parenchyma. The heart was enlarged (620 g) and showed changes associated with chronic ischemic heart disease: severe stenosis of native coronary arteries (left anterior descending, left circumflex, and right main coronary arteries), patent graft vessels, and moderately extensive replacement-type interstitial fibrosis. Aside from the aforementioned findings, the gross and microscopic examinations of remaining organs/tissue did not reveal significant findings. Lower levels of SARS-CoV-2 RNA were detected in sections of spleen, heart, intestine, liver, and skeletal muscle. SARS-CoV-2 RNA was not detected in samples of esophagus, stomach, kidney, adrenal, and skin samples (Table 1). Sequencing of the extracted viral RNA from the lung showed that the virus derived from Claude A2a with G11083T (ORF1a L3606F) mutation Table 2.

In summary, the cause of death was SARS-CoV-2 infection occurring in the setting of metastatic carcinoma, diabetes, and chronic ischemic cardiomyopathy, leading to respiratory failure.

DOI: 10.1093/ajcp/aqaa091

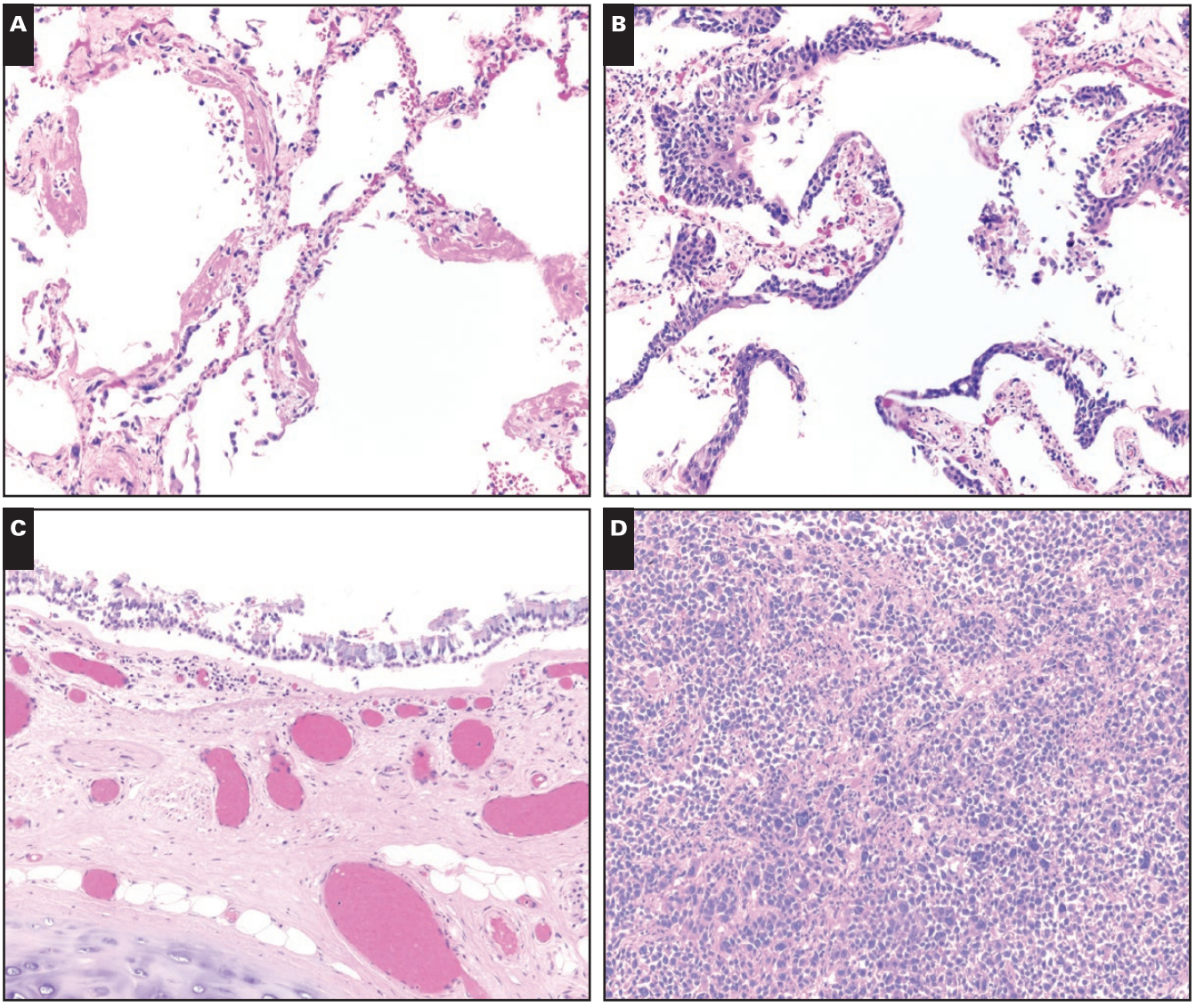

Image 2 (Case 1) Postmortem microscopic examination of the lungs showed diffuse alveolar damage characterized by hyaline membrane formation (**A**, ×100) and scattered squamous metaplasia of distal airways (**B**, ×100) on a background of emphysematous changes. Bronchial sampling showed only minimal submucosal chronic inflammation with unremarkable overlying respiratory epithelium (**C**, ×100), and the left lower lobe lung mass lesion was consistent with large cell carcinoma (**D**, ×100).

Case 2

The second decedent was a 54-year-old man with a history of hypertension and type 2 diabetes mellitus. He presented to a community hospital with an acute episode of shortness of breath, which worsened with exertion, and a generally dry cough of 2 days' duration. The patient denied having fever, headache, malaise, and gastrointestinal symptoms. He reported having never smoked. In the emergency department, his vital signs were notable for tachycardia (heart rate of 118 beats/min) and oxygen saturation of 76%. He was afebrile. Physical examination was notable for unlabored breathing with diminished, yet clear, breath sounds bilaterally, tachycardia, and good peripheral pulses. A chest roentgenogram showed diffuse bilateral airspace opacities with some areas of consolidation of the lower lungs, concerning for pneumonia **Image 3A**. The patient was admitted to the intensive care unit (ICU) with acute hypoxic respiratory failure, requiring 15 L/min of oxygen via nonrebreather mask. Initial labs showed an elevated d-dimer, and although there was some concern for pulmonary embolism, a CT scan was not pursued due to underlying renal function issues (elevated serum creatinine). Instead, empiric anticoagulation was initiated (heparin bridged to enoxaparin sodium). A nucleic amplification test performed on a nasopharyngeal swab sample came back positive for SARS-CoV-2 later the same night. Tests for influenza and respiratory syncytial virus were negative. On day 1 after admission,

DOI: 10.1093/ajcp/aqaa091

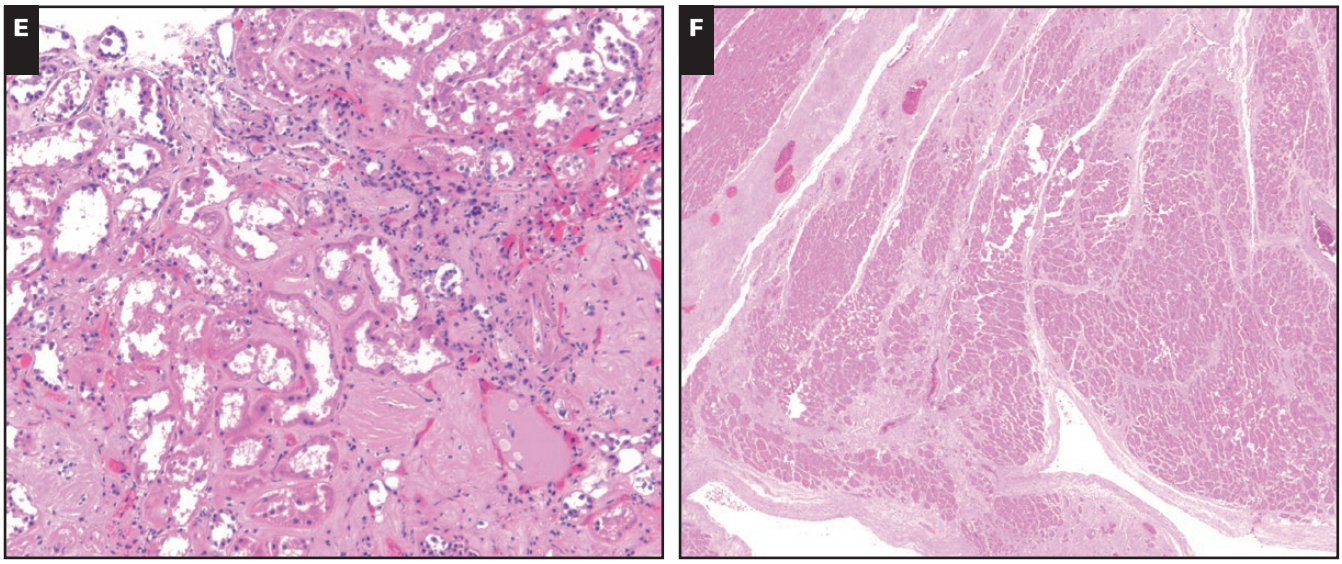

Image 2 (cont) The kidneys were notable for acute tubular injury on a background of moderately extensive chronic changes of the renal parenchyma (**E**, ×100). The heart showed sequelae of coronary artery atherosclerosis and chronic ischemic injury with replacement-type interstitial fibrosis (**F**, ×20).

Table 1
Molecular Detection of SARS-CoV-2 in Different FFPE Tissue Types

	Case 1				Case 2			
Tissue Sample	N1 Ct[a]	N2 Ct[a]	PCR[b]	cp/μL[c]	N1 Ct[a]	N2 Ct[a]	PCR[b]	cp/μL[c]
Lung	26.4	28.4	+	1000	29.5	32.3	+	100
Lymph node	31.0	32.2	+	100	30.9	32.2	+	10
Bronchus	30.6	32.7	+	100	37.3	39.4	+/–	1
Spleen	32.8	36.0	+	10	36.4	38.5	+/–	1
Heart	36.1	37.3	+/–	1	ND	ND	–	NA
Small intestine	ND	ND	+/–	<1	ND	ND	–	NA
Large intestine	ND	ND	+/–	<1	ND	ND	–	NA
Liver	37.9	39.4	+/–	<1	ND	ND	–	NA
Skeletal muscle	38.1	36.8	+/–	<1	ND	ND	–	NA
Esophagus	37.4	39.4	–	NA	ND	ND	–	NA
Stomach	ND	ND	–	NA	ND	ND	–	NA
Kidney	ND	ND	–	NA	ND	ND	–	NA
Adrenal	36.9	39.6	–	NA	ND	ND	–	NA
Skin	ND	ND	–	NA	ND	ND	–	NA

FFPE, formalin-fixed paraffin-embedded; NA, not applicable; ND, not done; SARS-CoV-2, severe acute respiratory syndrome coronavirus 2.
[a]Samples with cycle threshold (Ct) values <40 were considered positive.
[b]Polymerase chain reaction (PCR) noted as + when both N1 and N2 ≤ 36, and denoted as +/– when both >36 to 40.
[c]Approximate RNA copies per uL is given based on standard controls.

the patient was consented and enrolled in a trial to study the utility of the antiviral medication Remdesivir in treating SARS-CoV-2-infected patients. He received his first dose of the 10-day course the same day. Over the next few days, the patient's renal function showed improvement, but he still remained hypoxic despite escalation in oxygen therapy. A repeated chest roentgenogram performed 4 days after admission showed increased opacities bilaterally with a more consolidative appearance at the right lung base. Blood and urine cultures grew coagulase-negative *Staphylococcus* and *Enterococcus faecalis*, respectively, and the patient was started on antibiotics (vancomycin and piperacillin/tazobactam). The patient's WBC count also increased significantly over time, with a shift to increased absolute neutrophil counts and immature precursors in the peripheral blood. Lymphopenia was present beginning on day 2 of admission. A respiratory culture had no growth of bacteria or fungi. Serial chest roentgenograms showed initial worsening of his lung disease to more severe diffuse interstitial infiltrates **Image 3B** with subsequent stabilization of his imaging. He had increasing oxygen requirements beginning on day 9 after admission, and, despite appropriate therapy, continued to have low oxygen saturation.

DOI: 10.1093/ajcp/aqaa091

Table 2
Variants Detected in SARS-CoV-2 Genome From Case 2 FFPE Postmortem Lung Tissue[a]

Gene	Nucleotide Variation	Amino Acid Change	Mutation Type
ORF1a	1059 C>T	T265I	Missense
ORF1a	3037 C>T		Synonymous
ORF1a	9515 C>T	L3083I	Missense
ORF1a	11083 G>T	L3606F	Missense
ORF1a	12137_12142delGCTACT	A3958_T3959delAT	In-frame deletion
ORF1b	14408 C>T	P314L	Missense
S	23403 A>G	D614G	Missense
S	23778 C>T	T739I	Missense
ORF3a	25563 G>T	Q57H	Missense

FFPE, formalin-fixed paraffin-embedded; SARS-CoV-2, severe acute respiratory syndrome coronavirus 2.
[a]The common Clade A2a 5'UTR mutation 241C>T cannot be assessed in this sample due in lack of coverage from nucleotide positions 230 to 480.

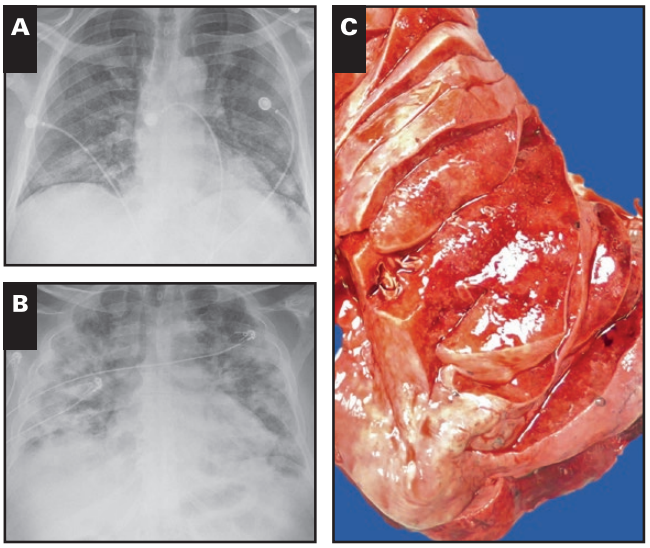

Image 3 (Case 2) Chest roentgenogram performed on the day of admission revealed diffuse bilateral airspace opacities with some areas of consolidation in the lower lungs, consistent with pneumonia (**A**). Chest roentgenogram performed on day 10 of hospital admission (1 day prior to death) showed extensive multifocal patchy infiltrates throughout the lungs bilaterally (**B**). Postmortem gross examination of bilateral lung showed congested and firm parenchyma (**C**).

Laboratory assessments around this time were notable for rapidly rising serum creatinine and liver enzymes. As a result of continued oxygen requirements, he was intubated on day 10 and also started on propofol with subsequent drop in blood pressure. Intravenous fluid resuscitation and pressor medications were started. The patient's oxygen saturation still showed no improvement, so a cisatracurium besylate drip was started and the patient was transferred to our institution for further management. While a central line was being placed, the patient became bradycardic with a heart rate of 30 beats/min. An arterial blood gas test at the time showed respiratory and metabolic acidemia. Despite further medication, the patient's heart rate continued to decrease to approximately 20 beats/min without a measurable blood pressure. The patient entered pulseless electrical activity arrest and resuscitative measures were initiated, with return of spontaneous circulation in approximately 2 min. The patient was evaluated for possible extracorporeal membrane oxygenation; however, he was deemed to be a poor candidate by the shock team. Ventilator settings at the time were as follows: positive end-expiratory pressure, 15 cm H_2O; fraction of expired O_2, 100%; and respiratory rate, 20 breaths/min. Despite continued ICU support, the patient died 10 days after admission to the hospital and 12 days after first reported onset of symptoms. The autopsy was limited to examination of the chest and abdomen only, per the family's request. The autopsy was performed 39 hours after death.

At postmortem examination, external findings were primarily limited to those of medical interventions such as intubation and central line placement. The decedent was overweight, bordering on obese, with a body mass index of 29.9 kg/m^2. In situ examination was significant for bilateral serosanguineous pleural effusions of 300 mL within each hemithorax. Grossly, bilateral lungs were strikingly heavy (right lung, 2,050 g; left lung, 1,100 g) with a congested appearance. Sectioning revealed a diffuse and relatively uniform firmness to the parenchyma **Image 3C**. There were no focal lesions. Histologically, sections from all lobes of the lungs showed varying stages of DAD with some areas demonstrating prominent hyaline membrane formation and significant pneumocyte hyperplasia (acute/exudative stage) **Image 4A** and others exhibiting patchy to diffuse intra-alveolar fibroblastic proliferation and interstitial edema (organizing stage) **Image 4B**. Areas of marked intra-alveolar acute inflammation were also present focally involving all lobes except the left lower lobe, diagnostic of acute bronchopneumonia **Image 4D**.

Varying degrees of pulmonary edema, clusters of multinucleated giant cells **Image 4C**, and foci of squamous metaplasia were also noted scattered throughout the lung parenchyma. Of note, despite extensive sampling and microscopic review, microthrombi were not identified.

DOI: 10.1093/ajcp/aqaa091

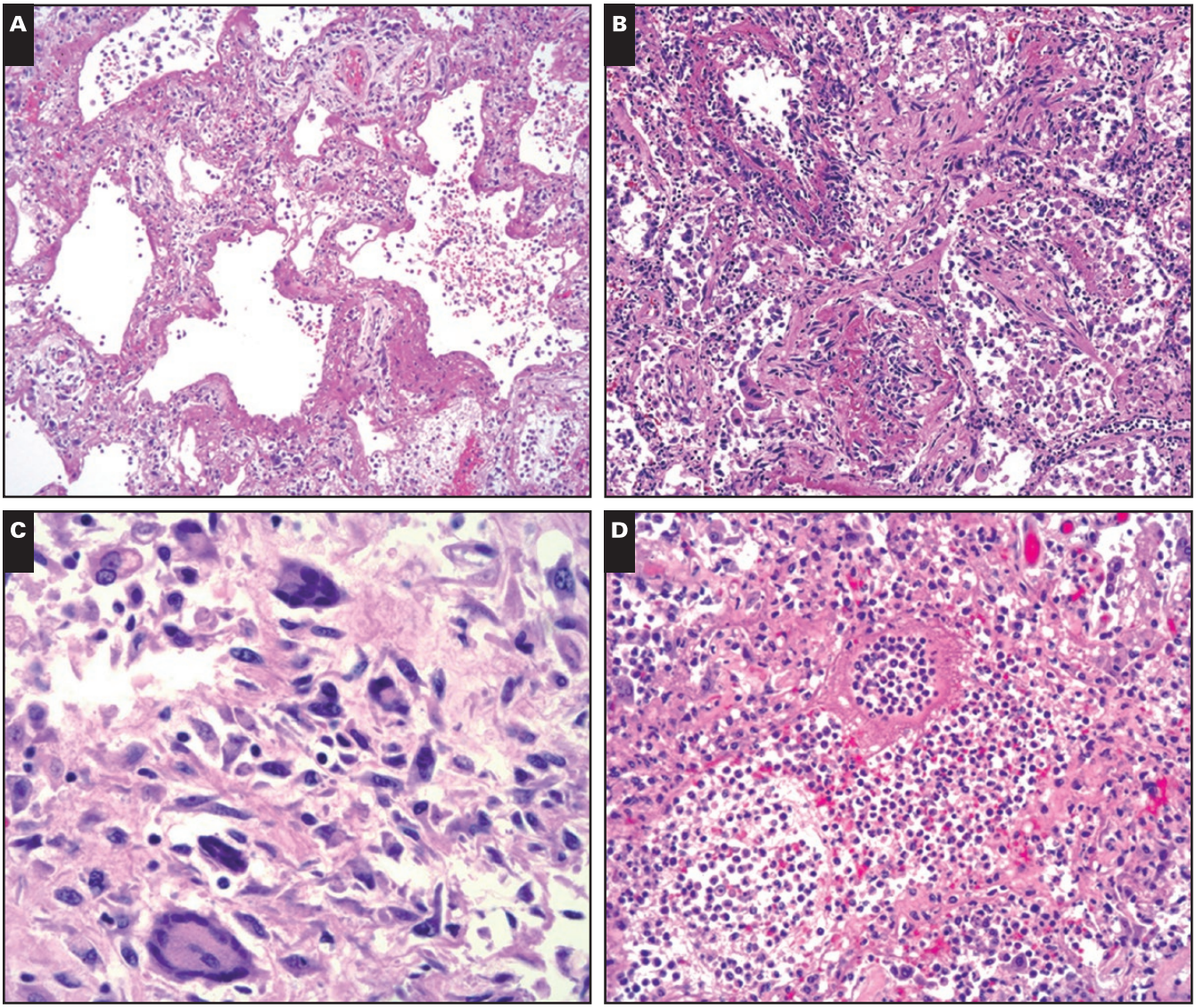

Image 4 (Case 2) Postmortem microscopic examination of the lungs revealed varying stages of diffuse alveolar damage characterized by extensive hyaline membrane formation (acute/exudative stage) (**A**, ×100) and intra-alveolar fibrin deposition (organizing stage) (**B**, ×100). Scattered multinucleated giant cells were also seen (**C**, ×400). The patient also had significant superimposed bronchopneumonia (**D**, ×200).

Submitted sections of the trachea **Image 4E** and proximal bronchi showed no significant abnormalities.

Additional significant findings noted at autopsy included evidence of diabetic glomerulosclerosis and acute tubular necrosis within bilateral kidneys **Image 4F**, an enlarged heart (560 g) with left ventricular hypertrophy, mild calcified atherosclerotic coronary artery disease, liver (2,300 g) and spleen (270 g) were enlarged secondary to acute congestion, and necrotizing granulomata within a right peribronchial lymph node and the spleen. A Grocott methenamine silver stain performed on the section of lymph node revealed yeast organisms most consistent with incidental *Histoplasma capsulatum*.

SARS-CoV-2 RNA was detected in sections of lung parenchyma, bronchi, lymph node, and spleen (Table 1). The presence of SARS-CoV-2 RNA was not detected in the heart, esophagus, stomach, intestines, liver, skeletal muscle, kidney, adrenal gland, or skin in case 2 (Table 1). Attempts at viral genome sequencing did not produce adequate coverage for successful genomic evaluation in this case, possibly due to low viral titers resulting from Remdesivir administration.

In summary of these findings, the cause of death was SARS-CoV-2 infection occurring in the setting of diabetes and underlying cardiovascular disease leading to respiratory and subsequent multiorgan system failure.

DOI: 10.1093/ajcp/aqaa091

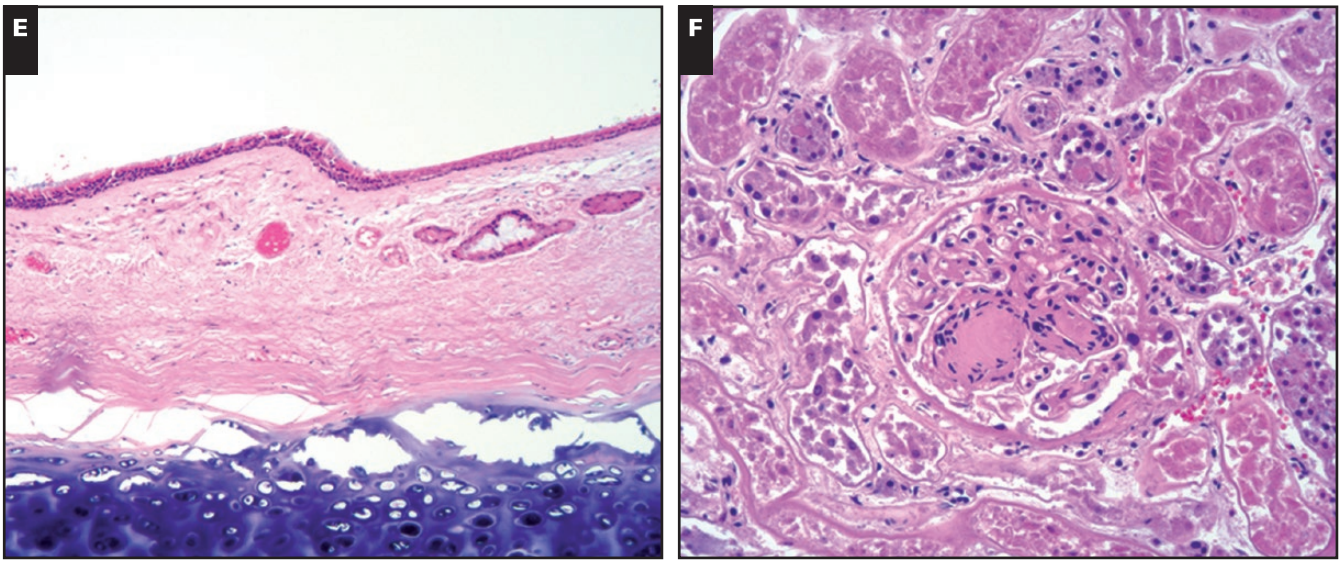

Image 4 (cont) Tracheal sampling showed only minimal submucosal chronic inflammation with unremarkable overlying respiratory epithelium (**E**, ×100). The kidneys were notable for acute tubular necrosis on a background of diffuse and nodular diabetic glomerulosclerosis (**F**, ×200).

Discussion

Here we report the detection of SARS-COV-2 RNA in a wide range of organs similar to that reported by an investigation of cases from Washington State.[7] This is the first study to our knowledge to demonstrate SARS-COV-2 RNA detection in several major organs and to sequence SARS-COV-2 genome from postmortem FFPE sections.

SARS-CoV-2 and SARS-CoV use spike (S) proteins to bind to the host cell via angiotensin converting enzyme 2 (ACE2) as an entry receptor leading to the internalization of the complex by the host cell.[8-11] ACE2, a counterregulatory component of the renin angiotensin aldosterone system, is mainly localized in the heart, kidney, endothelium, and testis, but is also expressed at low levels in many other tissues such as the brain, intestines, and lung.[11] In this study, we detected SARS-CoV-2 RNA in a number of ACE2 expressing tissues including lungs, heart, and intestines. We were also able to detect viral RNA from FFPE samples from upper airways, lymph node, spleen, and liver, which mirrors the finding of prior reports with analysis from fresh tissue.[7,12] Although virus RNA was detected in extrapulmonary tissues, there was no histomorphologic evidence of acute pathologic changes attributable to the virus itself or an inflammatory response.

Although relatively few reports documenting postmortem pathologic findings in patients with SARS-CoV-2 have been published to date, specific patterns of injury have emerged. As is expected in the clinical setting of pneumonia and ARDS, the lungs have been found to be the most consistently and severely affected. Several reports have demonstrated features of DAD, primarily in the acute or exudative phase in the majority of autopsies performed.[2,3,8,13] These have been characterized by intra-alveolar fibrin with associated hyaline membrane formation, markedly reactive pneumocytes, and variable squamous metaplasia. Fewer cases showed more advanced changes associated with DAD, including intra-alveolar fibroblastic proliferation and interstitial edema.[8,13] Additional findings that have been frequently noted include multinucleated giant cells,[3,8,13] acute inflammation in the form of bronchopneumonia and/or acute bronchiolitis, and relative paucity of chronic inflammatory cells.[2,8,11] Both of our cases exhibited features of the acute phase of DAD, while case 2 showed more prominent organization. In case 1, these features were superimposed on a background of chronic emphysematous changes and in the setting of concomitant large cell carcinoma of the left lung with associated ipsilateral nodal metastasis. Additional pulmonary findings in case 2 included significant superimposed acute bronchopneumonia and several clusters of multinucleated giant cells.

Both patients also demonstrated histopathologic features of acute renal injury superimposed on a background of moderate chronic changes to the renal parenchyma, in keeping with their histories of diabetes mellitus and hypertension. Case 2 exhibited classic features of nodular diabetic glomerulosclerosis. Both patients also demonstrated congestive splenomegaly and

DOI: 10.1093/ajcp/aqaa091

sinusoidal congestion of the liver. While these features have also been mentioned in other reports,[2,13] they may simply be related to terminal changes in these acutely ill patients rather than a direct result of the viral infection. Also in keeping with the reported literature, the additional pathologic changes identified in our cases were associated with the patients' underlying chronic medical conditions and did not seem to be specifically related to SARS-CoV-2 infection. For example, case 1 showed advanced cardiovascular disease as evidenced by cardiomegaly, severe atherosclerotic coronary artery disease, and remote ischemic changes within the myocardium. Cardiomegaly without significant coronary artery disease or evidence of ischemic injury was seen in case 2. Neither heart showed features of lymphocytic myocarditis, which has been reported as a possible consequence of SARS-CoV-2 infection.[8] Additionally, although several anecdotal reports regarding hypercoagulability have also begun circulating, histologic documentation of microthrombi has only rarely been reported in the published literature.[2] We were unable to identify any microthrombi in our 2 patients. Gross and histopathologic examination of the upper respiratory tract (main bronchi and trachea), pancreas, adrenal glands, gastrointestinal tract tissues, urinary bladder, skin, and skeletal muscle in our cases showed no significant changes.

Other postmortem ancillary studies have been performed on SARS-CoV-2 patients. Localization studies of SARS-CoV-2 by immunofluorescence revealed prominent expression on alveolar epithelial cells, including damaged, desquamated cells within the alveolar space.[4] Ultrastructural examination by electron microscopy was able to locate viral particles in type II pneumocytes, upper airway and intestinal mucosal epithelial cells, and proximal tubular epithelial cells.[7] Tian et al[12] performed reverse transcriptase polymerase chain reaction (RT-PCR) for SARS-CoV-2 on postmortem FFPE core biopsies collected from 4 patients and reported detection of SARS-CoV-2 RNA in heart, lung, and liver in at least 1 patient in their cohort. In our study we were able to consistently detect the virus in lung and lymph node samples, while bronchus samples also contained viral RNA, but at lower relative concentration compared to lung tissue. It has been postulated that moderate levels of RNA in lymph nodes reflect viral presence in leukocytes that may serve as a route for the virus to disseminate from airways or lung parenchyma to other organs.[7] Similarly, in an autopsy study performed on macaques on day 4 post infection, the highest SARS-CoV-2 RNA levels were detected in lungs, using quantitative RT-PCR. Viral RNA was also detected in the lymph nodes in 3 out of 4 animals.[13]

Monitoring the spread of virus in a pandemic is critical in disease control. Shared SARS-CoV-2 genotyping efforts and resources like the Global Initiative on Sharing All Influenza Data (GISAID, https://www.gisaid.org), NextStrain (https://nextstrain.org), and Johns Hopkins University Dashboard (https://coronavirus.jhu.edu/map.html) have enabled dynamic tracking of the evolution of the pandemic, enhanced monitoring of infection patterns, and have allowed better estimations of the affected population size in communities.[14] Like other RNA viruses, the RNA-dependent RNA polymerase of SARS-CoV-2 lacks proofreading capability, leading to an accumulation of mutations in its genome over time. Mutations in the critical proteins, including the S protein, RNA polymerase, RNA primase, and nucleoprotein, have been discovered.[15,16] These mutations are not equally distributed across the genome and generate hotspots that can be linked to specific geographic location of the outbreak. Knowledge and monitoring of these mutation sites is critical in designing a vaccine for preventing the infection as well as therapies for treatment of SARS-CoV-2.[14,17] Further studies showing the effect of these mutations on pathogenicity and pathobiology of the virus are needed.

Sequencing of viral RNA from FFPE lung tissue from the case 1 autopsy showed mutations most consistent with a subset of the Western European Clade A2a (C3037T, C14408T, A23403G),[16] with mutations enriched in New York State A2a cases (C1059T and G25563T).[15] The viral RNA from our cases also had G11083T mutation that to date has been described in only 2% (13/648) of the A2a clade that contain C1059T mutation. It has been suggested that the G11083T mutation is more common in regions (Italy and Brazil) with higher fatality rates.[18] The G11083 mutation was described in the first case of SARS-CoV-2 in Italy.[19] A study examining the transmission and evolution of SARS-CoV-2 in cruise quarantine suggests that the G11083T mutation can be transmitted via RNA recombination.[20] Linkage disequilibrium analysis suggests that RNA recombination with a G11083T mutation may contribute to the increase of mutations among the viral progeny.[20] In this case we did observe other mutations not extensively described in previous genomic sequencing efforts, including point mutations C9515T, C23378T, and in-frame deletion 12137_12142del (Table 2). More studies are needed to determine if G11083T, or other mutations detected in this case, may increase the fitness of the carrier virus as a benefit allele in the future.

The challenge that pathologists and the medical community at large face is determining if deaths in individuals who present with the clinical signs and symptoms of SARS-CoV-2 infection are truly infected with the virus. It is not standard for all autopsies to take swabs or put aside fresh tissue for potential

DOI: 10.1093/ajcp/aqaa091

molecular testing for SARS-CoV-2 detection, whereas production of FFPE tissue blocks is standard for most autopsies that require histologic examination. The ability to detect SARS-CoV-2 RNA from FFPE tissue may assist in cases in which there are clinical, or even histologic, findings that overlap findings found in SARS-CoV-2 infection. FFPE blocks are stored on many autopsies in many places from the period preceding the recognized onset of community-acquired SARS-CoV-2 infection. Recent reports suggest that SARS-CoV-2 infection has been detected in cases that preceded the previously recognized onset of community transmission in the United States. Our results suggest that sequencing of FFPE materials could contribute to a greater understanding of the early onset and spread of SARS-CoV-2 infection in the United States or other countries.

Possible limitations for molecular testing on autopsy samples include sampling bias if virus involvement is focal. This can be addressed by obtaining multiple samples from each organ. Our results showed widespread positivity of samples throughout sites in the lung and airways. This study supports sampling of upper and lower airways, immune organs (lymph node and spleen), and to a lesser degree the intestine, heart, and liver. Another concern is postmortem tissue autolysis and RNA degradation. Further studies are required to determine the stability of viral RNA in different organs after death. Finally, since the virus may affect each organ differently, individual organs may be expected to have different viral loads at any given time in the course of the disease. However, the clinical correlation of such findings is yet to be determined.

In conclusion, the findings of our postmortem examinations support major histopathologic features previously reported in the literature, the most striking of which is DAD. Changes in other organs, like the kidneys and heart, are likely secondary or related to underlying diseases. As might be expected given this pattern of injury, SARS-CoV-2 RNA is more easily detected in lung and upper airway tissue when compared to other organs. Interestingly, our study also documents detection in hematopoietic and lymphoid organs (lymph node and spleen) and may lend credence to the theory that leukocytes could serve as a route for dissemination of the virus from airways to other organs.[8] We propose that detection of SARS-CoV-2 RNA from postmortem FFPE tissues from multiple sites can aid in tracking the spread of the novel coronavirus and in gaining a better understanding of its pathophysiologic effects on human health. Additionally, the retrospective sequencing of archived FFPE material may allow for more definitive determination of the rate of prevalence of SARS-CoV-2 infection and therefore providing more accurate epidemiologic data on the virus's course and entry into a given population.

Corresponding author: Navid Sadri, MD, PhD; navid.sadri@uhhospitals.org.

**First authors.*

References

1. Zhu N, Zhang D, Wang W, et al; China Novel Coronavirus Investigating and Research Team. A novel coronavirus from patients with pneumonia in China, 2019. *N Engl J Med.* 2020;382:727-733.
2. Barton LM, Duval EJ, Stroberg E, et al. COVID-19 autopsies, Oklahoma, USA. *Am J Clin Pathol.* 2020;153:725-733.
3. Xu Z, Shi L, Wang Y, et al. Pathological findings of COVID-19 associated with acute respiratory distress syndrome. *Lancet Respir Med.* 2020;8:420-422.
4. Zhang H, Zhou P, Wei Y, et al. Histopathologic changes and SARS-CoV-2 immunostaining in the lung of a patient with COVID-19. *Ann Intern Med.* 2020;172:629-632.
5. Rhoads DD, Cherian SS, Roman K, et al. Comparison of Abbott ID Now, Diasorin Simplexa, and CDC FDA EUA methods for the detection of SARS-CoV-2 from nasopharyngeal and nasal swabs from individuals diagnosed with COVID-19. *J Clin Microbiol.* 2020. doi: 10.1128/JCM.00760-20
6. Hadfield J, Megill C, Bell SM, et al. Nextstrain: real-time tracking of pathogen evolution. *Bioinformatics.* 2018;34:4121-4123.
7. Bradley BT, Maioli H, Johnston R, et al. Histopathology and ultrastructural findings of fatal COVID-19 infections. Preprint at https://wwwmedrxivorg/content/101101/2020041720058545v1.
8. Li F, Li W, Farzan M, et al. Structure of SARS coronavirus spike receptor-binding domain complexed with receptor. *Science.* 2005;309:1864-1868.
9. Zhang H, Penninger JM, Li Y, et al. Angiotensin-converting enzyme 2 (ACE2) as a SARS-CoV-2 receptor: molecular mechanisms and potential therapeutic target. *Intensive Care Med.* 2020;46:586-590.
10. Hoffmann M, Kleine-Weber H, Schroeder S, et al. SARS-CoV-2 cell entry depends on ACE2 and TMPRSS2 and is blocked by a clinically proven protease inhibitor. *Cell.* 2020;181:271-280.e8.
11. Hamming I, Timens W, Bulthuis ML, et al. Tissue distribution of ACE2 protein, the functional receptor for SARS coronavirus: a first step in understanding SARS pathogenesis. *J Pathol.* 2004;203:631-637.
12. Tian S, Xiong Y, Liu H, et al. Pathological study of the 2019 novel coronavirus disease (COVID-19) through postmortem core biopsies. *Mod Pathol.* 2020. doi: 10.1038/s41379-020-0536-x
13. Rockx B, Kuiken T, Herfst S, et al. Comparative pathogenesis of COVID-19, MERS, and SARS in a nonhuman primate model. *Science.* 2020.
14. Forster P, Forster L, Renfrew C, et al. Phylogenetic network analysis of SARS-CoV-2 genomes. *Proc Natl Acad Sci U S A.* 2020;117:9241-9243.
15. Butler DJ, Mozsary C, Meydan C, et al. Host, viral, and environmental transcriptome profiles of the severe acute respiratory syndrome coronavirus 2 (SARS-CoV-2). Preprint at https://wwwbiorxivorg/content/101101/2020042004 8066v4.

16. Wang JT, Lin YY, Chang SY, et al. The role of phylogenetic analysis in clarifying the infection source of a COVID-19 patient. *J Infect.* 2020.
17. Xu X, Chen P, Wang J, et al. Evolution of the novel coronavirus from the ongoing Wuhan outbreak and modeling of its spike protein for risk of human transmission. *Sci China Life Sci.* 2020;63:457-460.
18. Banerjee S, Dhar S, Bhattacharjee S, et al. Decoding the lethal effect of SARS-CoV-2 (novel coronavirus) strains from global perspective: molecular pathogenesis and evolutionary divergence. Preprint at https://wwwbiorxivorg/content/101101/2020200406027854v1.
19. Capobianchi MR, Rueca M, Messina F, et al. Molecular characterization of SARS-CoV-2 from the first case of COVID-19 in Italy. *Clin Microbiol Infect.* 2020. doi: 10.1016/j.cmi.2020.03.025
20. Yeh TY, Contreras GP. Faster de novo mutation of SARS-CoV-2 in shipboard quarantine. *Bull World Health Organ.* E-pub: April 6, 2020. doi: 10.2471/BLT.20.255

DOI: 10.1093/ajcp/aqaa091